2011 American Control Conference
on O'Farrell Street, San Francisco, CA, USA
June 29 - July 01, 2011

Robust Vibration Isolation of a 6-DOF System Using Modal Decomposition and Sliding Surface Optimization

Chenyang Ding, A.A.H. Damen, P.P.J. van den Bosch

***Abstract*— For a high-performance 6-DOF Active Vibration Isolation System (AVIS), the vibration isolation performance (transmissibility) is the most important criterion and the disturbance rejection performance (compliance) has lower priority. The strategy of combining modal decomposition and frequency-shaped sliding surface control is applied based on the measurement scheme of relative displacement and payload absolute acceleration. Modal decomposition decouples the six modes and calculates the equivalent sensor noises for each mode. The designed performances, transmissibility and sensitivities to the two sensor noises, depend solely on the sliding surface design. The sliding surface is optimized for each mode with predefined constraints which are derived from common industrial requirements. The regulator is designed to realize the designed transmissibility for each mode and to achieve low compliance. The numerical example of the sliding surface optimization gives better result than the manual design. This strategy designs the four performances step by step and iterative design is not necessary.**

I. Introduction

In the semiconductor industry, wafer scanners used to produce integrated circuits, demand an Active Vibration Isolation System (AVIS) with six Degrees-Of-Freedom (DOF) to support and to inertially fix the payload despite of all disturbances, including floor vibrations and directly applied forces. As integrated circuit details up to nanometer accuracy are being written with a light source, the requirements posted on the AVIS are quite demanding. The payload of such an AVIS weights a few thousand kilograms. The 6-DOF AVIS based on pneumatic isolators [8], which compensates the payload gravity by pressurized air, is currently applied in the industry. The 6-DOF AVIS based on electromagnetic isolators, which compensates the payload gravity by passive permanent magnetic force, is also feasible [9] and being investigated [2] as an alternative.

The objective of the AVIS control is to minimize the payload absolute displacement (the terminology *absolute* indicates that this physical variable is with respect to an inertially fixed reference). However, neither floor absolute displacement nor payload absolute displacement is directly measurable by any industrial sensors. Integration of absolute velocity/acceleration signal is not feasible because of the limited performance of the industrial sensors. Therefore, the relative displacement (payload displacement with respect to the floor) and the payload absolute acceleration [1], [11] are measured for control. The AVIS control methodology based on this measurement scheme is studied to achieve both vibration isolation and direct disturbance force rejection.

The conventional strategy [11] is to apply the skyhook control [5] to the decoupled system. The skyhook control is able to reduce or even remove the resonance peak but vibration isolation improvement at low frequencies is difficult. The H_∞ control [1] can be directly applied to solve the Multi-Input-Multi-Output (MIMO) problem. It depends on the weighting filters design to optimize the closed-loop performance. But this design process is complicated and usually requires many iterations to complete. Besides, the H_∞ controller usually has high order which limits its application.

A strategy combining modal decomposition and the frequency-shaped sliding surface control based on the measurement scheme of relative displacement and payload absolute velocity has been proposed [4]. Robust skyhook performance is experimentally validated using a 1-DOF setup. But the sliding surface design is based on ideal feedback signals wherein neither sensor noises nor sensor dynamics are considered. In our previous work [3], the pole placement method is proposed to design the sliding surface but manual pole placement is quite cumbersome.

In this paper, the sliding surface is designed by solving an optimization problem, which is formulated according to vibration isolation requirements, floor vibration strength, and sensor performances. Both optimized vibration isolation performance and disturbance rejection are to be realized by the regulator design. The 6-DOF AVIS model, the sensor models, modal decomposition, and the performance requirements are described in Section II. The frequency-shaped sliding surface control is described more generally in Section III. The sliding surface design by optimizing the vibration isolation is given in Section IV. This work is concluded in Section V.

II. Problem Statement

A. 6-DOF AVIS Model

The simplified schematic of the AVIS in a wafer scanner is illustrated in Fig. 1. The base-frame is mounted on the floor. We assume that the payload, the base-frame, and all mounting connections are rigid. The payload absolute displacement vector and the relative displacement vector are denoted by ${}^{e}\overrightarrow{q}$ and ${}^{b}\overrightarrow{q}$, respectively. They are defined as

$$ {}^{e}\overrightarrow{q} = [{}^{e}q_x, {}^{e}q_y, {}^{e}q_z, {}^{e}q_\phi, {}^{e}q_\theta, {}^{e}q_\psi]^T, \tag{1} $$

$$ {}^{b}\overrightarrow{q} = [{}^{b}q_x, {}^{b}q_y, {}^{b}q_z, {}^{b}q_\phi, {}^{b}q_\theta, {}^{b}q_\psi]^T, \tag{2} $$

where the subscript x, y, and z denote the three Cartesian axes and ϕ, θ, and ψ denote the roll, pitch, and yaw rotations. The superscripts e and b denote the coordinate systems fixed to an inertial fixed reference and the base-frame, respectively. The two vectors are related by

$$ {}^{b}\overrightarrow{q} = {}^{e}\overrightarrow{q} - {}^{e}\overrightarrow{\rho}, \tag{3} $$

978-1-4577-0079-8/11/$26.00 ©2011 AACC

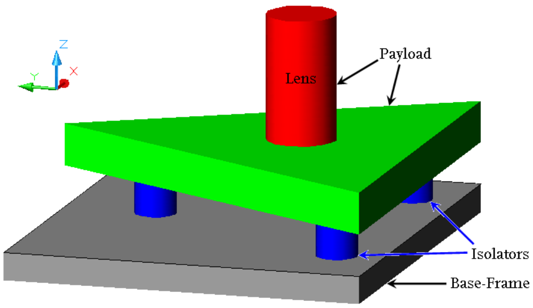

Fig. 1. Simplified schematic of the 6-DOF AVIS in a wafer scanner.

where ${}^{e}\vec{\rho}$ is the base-frame displacement vector. The control input to the 6-DOF AVIS is denoted by a wrench vector

$$\vec{w_a} = [f_{ax}, f_{ay}, f_{az}, t_{a\phi}, t_{a\theta}, t_{a\psi}]^T, \tag{4}$$

where f denotes the force and t denotes the torque. The disturbance wrench vector is denoted by $\vec{w_d}$. Each isolator can be modeled by springs and dampers. The 6-DOF equation of motion for the payload has a linearized form

$$M^{e}\ddot{\vec{q}} + D^{b}\dot{\vec{q}} + K^{b}\vec{q} = \vec{w_d} - \vec{w_a}, \tag{5}$$

where M, D, and K are the mass matrix, the damping matrix, and the stiffness matrix, respectively. For the 6-DOF AVIS, we assume proportional damping: $D = \alpha M + \beta K$ (α and β are constants). The dashed rectangular in Fig. 2 shows the diagram of the 6-DOF model according to (5). I is the 6×6 identity matrix. The transformation matrices ${}^{m}\boldsymbol{T}_a$, ${}^{b}\boldsymbol{T}_s$, and ${}^{e}\boldsymbol{T}_s$ are determined by the allocations of the actuators, displacement sensors, and acceleration sensors, respectively. The subscripts/superscripts s and a denote the corresponding sensor spaces and the actuator space, respectively. The subscript/superscript m denote the coordinate system fixed to the payload. The three matrices can be calculated by geometry.

B. Sensor Models

The vectors ${}^{s}\widetilde{\vec{q}}$ and ${}^{s}\widetilde{\vec{a}}$ contains the output signals of the six displacement sensors and the six acceleration sensors, respectively. The vectors ${}^{s}\vec{q}$ and ${}^{s}\vec{a}$ denote the true displacement and acceleration signals, respectively. The displacement sensor usually have very high bandwidth (in the order of 10^4 Hz). For this reason, the sensor dynamics are negligible at the interested frequencies (up to the order of 100 Hz). The vector which contains the six displacement sensor noise, denoted by $\vec{n_q}$, is assumed to be independent of ${}^{s}\vec{q}$ so that ${}^{s}\widetilde{\vec{q}}$ is derived by

$${}^{s}\widetilde{\vec{q}} = {}^{s}\vec{q} + \vec{n_q}. \tag{6}$$

There are many types of acceleration sensors. The accelerometer based on piezoelectric effect is capable of acceleration measurement from zero frequency up to a certain resonant frequency ω_a (in the order of 10^3-10^4 Hz). At low frequencies, the sensor dynamics are negligible except there is usually a DC bias which can be classified as a part of the sensor noise. The accelerometer noise, denoted by $\vec{n_a}$, is

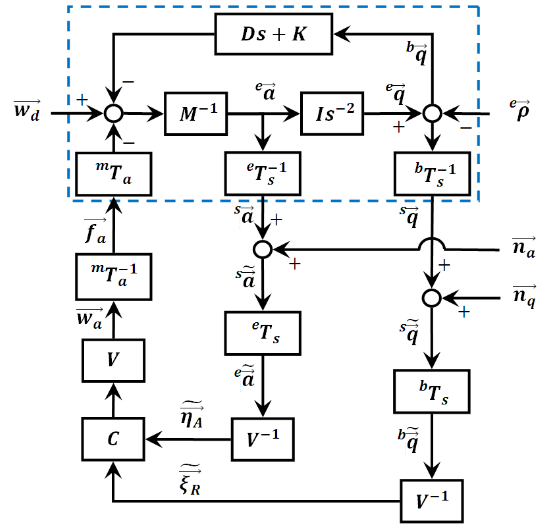

Fig. 2. Modal decomposition of the 6-DOF AVIS model.

assumed to be independent of ${}^{s}\vec{a}$. The relation between ${}^{s}\widetilde{\vec{a}}$ and ${}^{s}\vec{a}$ is

$${}^{s}\widetilde{\vec{a}} = {}^{s}\vec{a} + \vec{n_a}. \tag{7}$$

Both (6) and (7) are illustrated in Fig. 2.

C. Modal Decomposition

Modal decomposition of a multi-DOF AVIS is described in [4], [8]. Vibration isolation performance of an AVIS is significantly affected by the sensor dynamics and noises. This subsection describes the modal decomposition of a 6-DOF AVIS considering the sensor dynamics and noises.

Assume that M is non-singular, (5) is equivalent to

$${}^{e}\ddot{\vec{q}} + M^{-1}D^{b}\dot{\vec{q}} + M^{-1}K^{b}\vec{q} = M^{-1}\vec{w_d} - M^{-1}\vec{w_a}. \tag{8}$$

Apply the eigenvalue decomposition to the matrix $M^{-1}K$, we have

$$M^{-1}K = VWV^{-1}, \tag{9}$$

where V is a 6×6 matrix containing the linearly independent eigenvectors and W is a 6×6 diagonal matrix containing the corresponding eigenvalues. Define the modal coordinates $\vec{\xi_A} = V^{-1}{}^{e}\vec{q}$ and $\vec{\xi_R} = V^{-1}{}^{b}\vec{q}$, then (8) yields

$$\ddot{\vec{\xi_A}} + V^{-1}M^{-1}DV\dot{\vec{\xi_R}} + W\vec{\xi_R} = V^{-1}M^{-1}(\vec{w_d} - \vec{w_a}). \tag{10}$$

Substitute $D = \alpha M + \beta K$, $\vec{u_d} = V^{-1}M^{-1}\vec{w_d}$, and $\vec{u_a} = V^{-1}M^{-1}\vec{w_a}$ into (10), we have

$$\ddot{\vec{\xi_A}} + (\alpha I + \beta W)\dot{\vec{\xi_R}} + W\vec{\xi_R} = \vec{u_d} - \vec{u_a}. \tag{11}$$

Fig. 2 shows the control diagram of the 6-DOF AVIS with modal decomposition. The block C is a 6×6 diagonal transfer matrix to be designed. The equivalent diagram of Fig. 2 is shown in Fig. 3. The vector $\vec{\eta_A}$ is defined as the second time derivative of the vector $\vec{\xi_A}$. $\widetilde{\vec{\eta_A}}$ is the measured $\vec{\eta_A}$ with noises.

$$\widetilde{\vec{\eta_A}} = \vec{\eta_A} + \vec{e_\eta}, \text{ where } \vec{e_\eta} = V^{-1}{}^{e}\boldsymbol{T}_s\vec{n_a}. \tag{12}$$

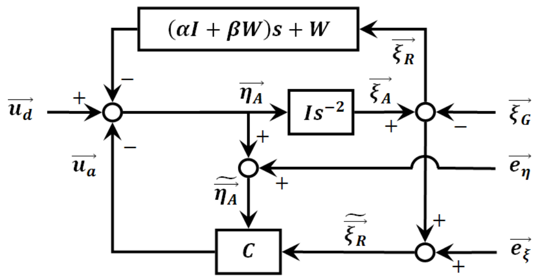

Fig. 3. Equivalent diagram of the modal decomposition.

The vector $\widetilde{\overrightarrow{\xi_R}}$ is the measured $\overrightarrow{\xi_R}$ with noises.

$$\widetilde{\overrightarrow{\xi_R}} = \overrightarrow{\xi_R} + \overrightarrow{e_\xi}, \text{ where } \overrightarrow{e_\xi} = V^{-1b}\boldsymbol{T}_s\overrightarrow{n_q}. \tag{13}$$

D. Performance Requirements

There are four closed-loop performances. The transmissibility $\mathbb{T}$ is the transfer from floor vibration to payload vibration. The compliance $\mathbb{C}$ is the transfer from the directly applied force to payload vibration. The sensitivity $\mathbb{S}$ is the transfer from the acceleration sensor noise to payload vibration. The sensitivity $\mathbb{R}$ is the transfer from the displacement sensor noise to the payload vibration. $\mathbb{S}$ and $\mathbb{R}$ are concerned because they would affect $\overline{|\mathbb{T}|}$, the upper bound of $|\mathbb{T}|$. All $\mathbb{T}$, $\mathbb{C}$, $\mathbb{S}$, and $\mathbb{R}$ for the 6-DOF AVIS are 6×6 transfer matrices. Since the modal decomposition would theoretically keep the off-diagonal entries zero, only the diagonal entries $\mathbb{T}_i$, $\mathbb{C}_i$, $\mathbb{S}_i$, and $\mathbb{R}_i$, $\forall\, i \in \{1,2,3,4,5,6\}$ are concerned. In this paper, i denotes the index of the six modes by default.

The fundamental constraints are

1. $\mathbb{T}_i$, $\mathbb{C}_i$, $\mathbb{S}_i$, and $\mathbb{R}_i$ are all stable.
2. Interested frequency range is from zero up to the order of 10^2 Hz.
3. $|\mathbb{T}_i(0)| = 1$ (0 dB).
4. $\frac{d|\mathbb{T}_i(\omega)|}{d\omega} \leq -40$ dB/dec at high frequencies.
5. $|\mathbb{S}_i(0)| = 0$ ($-\infty$ dB). This item is to filter the acceleration sensor DC bias.
6. $|\mathbb{C}_i(0)| = 0$ ($-\infty$ dB) is preferred.

For all $\mathbb{T}_i$, $\mathbb{C}_i$, $\mathbb{S}_i$, and $\mathbb{R}_i$, lower magnitude indicates better performance. For $\mathbb{T}_i$, lower cross-over frequency indicate better performance. Note that it is impossible to simultaneously improve all performances at a certain frequency. Among all the four performances, $\mathbb{T}_i$ is the most important one. As industrial environments usually have vibrations at a certain frequency, $\overline{|\mathbb{T}_i|}$ is required to be smaller than some desired value at these frequencies while its resonance peak is minimized. Based on these requirements, the optimized transmissibility is defined as follows.

Assume that the cut-off frequency of $\overline{|\mathbb{T}_i|}$, denoted by ω_c, has a required upper-bound, ω_1. Assume that ω_k and $\varepsilon_k, \forall\, k \in \{0,1,2,...,n\}$ are predefined constants that satisfy

- $\omega_0 < \omega_c$.
- $\omega_1 = \omega_c$.
- $\omega_k > \omega_c \;\forall\, k \in \{2,3,...,n\}$.
- $\varepsilon_0 > 1$.
- $\varepsilon_1 = 1$.
- $\varepsilon_k < 1 \;\forall\, k \in \{2,3,...,n\}$.

Let a denote a set of controller parameters to be designed. The transmissibility optimization is to find a set $\hat{a}$ which minimizes the resonance peak of the transmissibility upper bound under constraints.

$$\hat{a} = \min_a \sup_\omega \overline{|\mathbb{T}_i(\omega)|}, \tag{14}$$

under the constraints of

- $\overline{|\mathbb{T}_i(\omega)|} \leq \varepsilon_0, \forall\, \omega \leq \omega_0$.
- $\overline{|\mathbb{T}_i(\omega_k)|} \leq \varepsilon_k, \forall\, k \in \{1,2,...,n\}$.

Note that the above constraints are the most common industrial requirements for a particular AVIS. The objective of the AVIS control is to design the diagonal entries of the controller C as in Fig. 3 for each mode so that all the fundamental constraints are satisfied and the transmissibility is optimized.

III. Frequency-Shaped Sliding Surface Control

The name "frequency-shaped sliding surface" was given by K.D. Young and U. Ozguner [6] in 1993. It is usually applied to tracking control, in which, a measurable signal is to be minimized. It has been applied to AVIS control by L. Zuo and J.J.E. Slotine [4] in 2004. Therein, the sliding surface was designed for ideal absolute velocity signals. This section describes the optimal sliding surface design of a certain order based on the feedback scheme of relative displacement and absolute acceleration. The corresponding regulator design is also discussed.

The AVIS control methodology using frequency-shaped sliding surface takes two steps to design the controller C as in Fig 3. The diagram of the controller C is shown in Fig. 4. The first step is to design the frequency-shaped sliding surface, which is defined by the equation $\overrightarrow{\sigma_i} = 0$, where $\overrightarrow{\sigma} = [\sigma_1, \sigma_2, \sigma_3, \sigma_4, \sigma_5, \sigma_6]^T$. The blocks Λ_R and Λ_A are two transfer matrix designed to shape the sliding surface for the corresponding mode. The sliding surface design (Λ_R and Λ_A) determines the designed performances (the designed transmissibility $\mathbb{T}_d$, the designed accelerometer-noise sensitivity $\mathbb{S}_d$, and the designed displacement-sensor-noise sensitivity $\mathbb{R}_d$). The designed sliding surface and the original AVIS form a new system. The second step is to design the regulator R for this new system to keep $\overrightarrow{\sigma}$ zero and to fulfill the requirements of the compliance. As a result of the modal decomposition, all of these transfer matrices, Λ_R, Λ_A, $\mathbb{T}_d$, $\mathbb{S}_d$, $\mathbb{R}_d$, and R are 6×6 diagonal matrices. Their i^{th} diagonal entries are denoted by Λ_{Ri}, Λ_{Ai}, $\mathbb{T}_{di}$, $\mathbb{S}_{di}$, $\mathbb{R}_{di}$, and R_i, respectively. Subsection III-A describes how the sliding surface is related to the designed performances. Subsection III-B describes why the designed performances can be approximated to the closed-loop performances. The way to suppress the compliance is also provided.

A. Sliding Surface Design

This subsection describes how the designed performances ($\mathbb{T}_{di}$, $\mathbb{S}_{di}$, and $\mathbb{R}_{di}$) relate to the sliding surface Λ_{Ri} and Λ_{Ai}

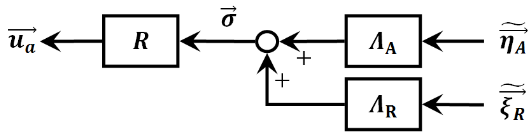

Fig. 4. Diagram of the frequency-shaped sliding surface controller.

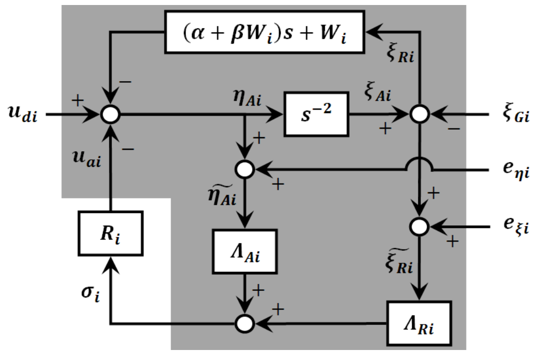

Fig. 5. Frequency-shaped sliding surface control diagram for the i^{th} mode.

for the i^{th} mode. The closed-loop control diagram for the i^{th} mode is shown in Fig. 5. Based on the signal loop,

$$\sigma_i = \Lambda_{Ai}(\eta_{Ai} + e_{\eta i}) + \Lambda_{Ri}(\xi_{Ri} + e_{\xi i}). \tag{15}$$

The equation $\sigma_i = 0$ is therefore equivalent to

$$\Lambda_{Ai}(\eta_{Ai} + e_{\eta i}) + \Lambda_{Ri}(\xi_{Ri} + e_{\xi i}) = 0. \tag{16}$$

Substitute $\eta_{Ai} = \xi_{Ai}s^2$ and $\xi_{Ri} = \xi_{Ai} - \xi_{Gi}$ into (16), we have

$$\frac{\Xi_{Ai}}{\Xi_{Gi}} = \frac{\Lambda_{Ri}}{\Lambda_{Ai}s^2 + \Lambda_{Ri}}\left(1 - \frac{E_{\xi i}}{\Xi_{Gi}}\right) - \frac{\Lambda_{Ai}}{\Lambda_{Ai}s^2 + \Lambda_{Ri}}\frac{E_{\eta i}}{\Xi_{Gi}}, \tag{17}$$

where Ξ_{Ai}, Ξ_{Gi}, $E_{\xi i}$, and $E_{\eta i}$ are the Laplace transforms of signals ξ_{Ai}, ξ_{Gi}, $e_{\xi i}$, and $e_{\eta i}$, respectively. The three designed performances, $\mathbb{T}_{di}$, $\mathbb{S}_{di}$, and $\mathbb{R}_{di}$ are defined as

$$\mathbb{T}_{di} = -\mathbb{R}_{di} = \frac{\Lambda_{Ri}}{\Lambda_{Ai}s^2 + \Lambda_{Ri}}, \qquad \mathbb{S}_{di} = \frac{-\Lambda_{Ai}}{\Lambda_{Ai}s^2 + \Lambda_{Ri}}. \tag{18}$$

According to (17), $|\mathbb{T}_{di}|$ has an upper bound, $\overline{|\mathbb{T}_{di}|}$:

$$\overline{|\mathbb{T}_{di}|} = |\mathbb{T}_{di}| + \left|\mathbb{R}_{di}\frac{E_{\xi i}}{\Xi_{Gi}}\right| + \left|\mathbb{S}_{di}\frac{E_{\eta i}}{\Xi_{Gi}}\right|. \tag{19}$$

All of $\mathbb{T}_{di}$, $\mathbb{S}_{di}$, and $\mathbb{R}_{di}$ can be realized by keeping σ_i zero, which is the task of the regulator R_i.

B. Regulator Design

The sliding surface and the original plant form a new system, P_{ni}, shown by the shaded blocks in Fig. 5. The input is u_{ai} and the output is σ_i. The transfer function is given by

$$P_{ni} = (\Lambda_{Ai}s^2 + \Lambda_{Ri})P_i, \text{ where } P_i = \frac{1}{s^2 + (\alpha + \beta W_i)s + W_i}. \tag{20}$$

Note that σ_i is a intermediate variable of the overall controller which is exactly known. The problem of keeping σ_i zero is a regulator problem, in which, the measurable output is to be kept zero. In [4], the switching control with a boundary layer design is applied to keep σ_i zero without any chatter. An adaptive algorithm is applied to deal with the plant parametric uncertainties. The adaptive algorithm is not necessary for the regulator design under the assumption that the plant parameters are known with reasonable accuracy. If the switching control is to be applied as the regulator, the boundary layer controller should be carefully designed to avoid the algebraic control loop. Since the boundary layer design relies on linear design tools [10], the regulator design stays in the linear framework no matter the switching control is applied or not. Therefore, the regulator R_i is assumed as a linear transfer function in this study. In this case, the closed-loop performances can be calculated.

The four closed-loop performances are calculated based on the diagram in Fig. 5.

$$\mathbb{T}_i = \frac{\Lambda_{Ri} + \frac{(\alpha+\beta W_i)s+W_i}{R_i}}{\frac{1}{P_iR_i} + \frac{(\alpha+\beta W_i)s+W_i}{R_i} + \Lambda_{Ai}s^2 + \Lambda_{Ri}}, \tag{21a}$$

$$\mathbb{C}_i = \frac{\frac{1}{R_i}}{\frac{1}{P_iR_i} + \frac{(\alpha+\beta W_i)s+W_i}{R_i} + \Lambda_{Ai}s^2 + \Lambda_{Ri}}, \tag{21b}$$

$$\mathbb{R}_i = \frac{-\Lambda_{Ri}}{\frac{1}{P_iR_i} + \frac{(\alpha+\beta W_i)s+W_i}{R_i} + \Lambda_{Ai}s^2 + \Lambda_{Ri}}, \tag{21c}$$

$$\mathbb{S}_i = \frac{-\Lambda_{Ai}}{\frac{1}{P_iR_i} + \frac{(\alpha+\beta W_i)s+W_i}{R_i} + \Lambda_{Ai}s^2 + \Lambda_{Ri}}. \tag{21d}$$

The upper bound of $|\mathbb{T}_i|$ due to the sensor noises, $\overline{|\mathbb{T}_i|}$, is calculated as

$$\overline{|\mathbb{T}_i|} = |\mathbb{T}_i| + \left|\mathbb{R}_i\frac{E_{\xi i}}{\Xi_{Gi}}\right| + \left|\mathbb{S}_i\frac{E_{\eta i}}{\Xi_{Gi}}\right|. \tag{22}$$

If the regulator has such a high gain that the conditions

$$\frac{1}{P_iR_i} + \frac{(\alpha+\beta W_i)s+W_i}{R_i} \ll \Lambda_{Ai}s^2 + \Lambda_{Ri}, \tag{23a}$$

$$\frac{(\alpha+\beta W_i)s+W_i}{R_i} \ll \Lambda_{Ri}. \tag{23b}$$

are valid, $\mathbb{T}_i$, $\mathbb{S}_i$ and $\mathbb{R}_i$ converges to $\mathbb{T}_{di}$, $\mathbb{S}_{di}$, and $\mathbb{R}_{di}$, respectively. Subsequently, (22) converges to (19). Further more, higher regulator gain also reduces $|\mathbb{C}_i|$. Note that the conditions (23) are required to be valid only at interested frequencies. The regulator gain has to be low at high frequencies to deal with possible unmodeled flexible modes.

IV. Optimized Sliding Surface

A. Sliding Surface Design

The two designed performances, $\mathbb{S}_{di}$ and $\mathbb{T}_{di}$ ($|\mathbb{T}_{di}| = |\mathbb{R}_{di}|$), depend solely on the sliding surface design (Λ_{Ri} and Λ_{Ai}) according to (18). The numerator polynomial and the denominator polynomial of Λ_j, $j \in \{Ai, Ri\}$ are denoted by N_j and D_j, $j \in \{Ai, Ri\}$, respectively. To satisfy the constraint of $\mathbb{S}_{di}(0) = 0$, N_{Ai} can be designed as $N_{Ai} = sN'_{Ai}$, where N'_{Ai} is another polynomial of s. Let $D_{Ai} = D_{Ri}$, (18) is simplified to

$$\mathbb{T}_{di} = \frac{N_{Ri}}{N'_{Ai}s^3 + N_{Ri}}, \qquad \mathbb{S}_{di} = \frac{sN'_{Ai}}{N'_{Ai}s^3 + N_{Ri}}. \tag{24}$$

If $\mathbb{T}_{di}$ is designed to have its lowest order, which is *three*, N'_{Ai} has to be a constant. Further more, the highest order of N_{Ri} is one if $|\mathbb{T}_{di}|$ has a decreasing rate of -40 dB/dec at high frequencies. $\mathbb{T}_{di}$ have the following form.

$$\mathbb{T}_{di} = \frac{a_1 s + a_0}{a_3 s^3 + a_1 s + a_0}, \text{ or } \mathbb{T}_{di} = \frac{a_0}{a_3 s^3 + a_0}, \tag{25}$$

where a_0, a_1, and a_3 are constant real numbers. In either case, it is difficult to find such a set of real numbers to make $\mathbb{T}_{di}$ stable.

If the order of $\mathbb{T}_{di}$ is designed to be *four*, $\mathbb{T}_{di}$ and $\mathbb{S}_{di}$ have the following form.

$$\mathbb{T}_{di} = \frac{a_2 s^2 + a_1 s + a_0}{a_4 s^4 + a_3 s^3 + a_2 s^2 + a_1 s + a_0}, \tag{26a}$$

$$\mathbb{S}_{di} = \frac{a_4 s^2 + a_3 s}{a_4 s^4 + a_3 s^3 + a_2 s^2 + a_1 s + a_0}, \tag{26b}$$

where a_k, $\forall\, k \in \{0,1,2,3,4\}$ are constant real numbers. They can be determined by choosing of the four stable poles of $\mathbb{T}_{di}$ and $\mathbb{S}_{di}$. If the order of $\mathbb{T}_{di}$ is further increased, the benefit is more flexibility to design the two performances and the trade-off is the increased order of the controller, which would subsequently increase the computation power.

B. Sliding Surface Optimization

The Power Spectrum Density (PSD) of the sensor noises ($\overrightarrow{n_q}$ and $\overrightarrow{n_a}$) can be experimentally measured [12] and subsequently used to calculate the PSD of sensor noises for each decomposed mode ($e_{\eta i}$ and $e_{\xi i}$). Similarly, the PSD of the base-frame acceleration can also be experimentally measured and subsequently used to calculate the PSD of equivalent base-frame displacement for each mode ($\eta_{Gi} = \ddot{\xi}_{Gi}$). The PSD ratios of the sensor noises over the base-frame displacement vary with the frequency. These variations can be described by two functions.

$$G_{\xi i}(\omega) = \frac{E_{\xi i}(\omega)}{\Xi_{Gi}(\omega)}, \; G_{\eta i}(\omega) = \frac{E_{\eta i}(\omega)}{\Xi_{Gi}(\omega)}. \tag{27}$$

Note that both $G_{\xi i}(\omega)$ and $G_{\eta i}(\omega)$ can be either transfer functions or look-up tables. (19) can be reformed to

$$\overline{|\mathbb{T}_{di}(\omega)|} = |\mathbb{T}_{di}(\omega)|(1 + |G_{\xi i}(\omega)|) + |\mathbb{S}_{di}(\omega)||G_{\eta i}(\omega)|. \tag{28}$$

There are two ways to parameterize the cost function $\overline{|\mathbb{T}_{di}(\omega)|}$. They are described as follows.

1) Pole Parameterization: Assume that $\mathbb{T}_{di}$ takes the form of (26), there are three possibilities of the four poles. Assume that $r_k < 0, \forall\, k \in \{1,2,3,4\}$ are independent real variables, the three possible combinations of the four stable poles are

- Four real poles (r_k, $\forall\, k \in \{1,2,3,4\}$).
- Two real poles (r_1 & r_2) and a conjugate pair ($r_3 \pm r_4 j$).
- Two conjugate pairs ($r_1 \pm r_2 j$ and $r_3 \pm r_4 j$).

In each case, $\overline{|\mathbb{T}_{di}(\omega)|}$ can be numerically calculated according to (28) and (26). The transmissibility optimization problem is formulated as follows.

To find the set of four negative variables $r_k, \forall\, k \in \{1,2,3,4\}$ which minimizes $\sup \overline{|\mathbb{T}_{di}(\omega)|}$ under constraints of

- $\overline{|\mathbb{T}_{di}(\omega)|} \le \varepsilon_0$, $\forall\, \omega \le \omega_0$.
- $\overline{|\mathbb{T}_{di}(\omega_k)|} \le \varepsilon_k$, $\forall\, k \in \{1,2,...,n\}$.

The above optimization problem can be solved numerically in Matlab for each case of pole combinations. The final optimal solution is the one with lowest $\sup \overline{|\mathbb{T}_{di}(\omega)|}$.

2) Denominator Parameterization: Assume that $\mathbb{T}_{di}$ takes the form of (26), the constants a_k, $\forall\, k \in \{0,1,2,3\}$ are used as parameters and the constant a_4 is set to one without losing generality. The transmissibility optimization problem is formulated as follows.

To find the set of four positive variables $a_k, \forall\, k \in \{0,1,2,3\}$ which minimizes $\sup \overline{|\mathbb{T}_{di}(\omega)|}$ under constraints of

- $\overline{|\mathbb{T}_{di}(\omega)|} \le \varepsilon_0$, $\forall\, \omega \le \omega_0$.
- $\overline{|\mathbb{T}_{di}(\omega_k)|} \le \varepsilon_k$, $\forall\, k \in \{1,2,...,n\}$.
- $a_k > 0$, $\forall\, k \in \{0,1,2,3\}$.
- $a_2 - a_1/a_3 > 0$.
- $a_1 - a_3 a_0/(a_2 - a_1/a_3) > 0$.

The last three constraints are used to keep $\mathbb{T}_{di}$ stable. They are derived using the Routh-Hurwitz criterion.

C. Numerical Example

A simple numerical example of the optimization process is given. Assume that

- $G_{\xi i}(\omega) = 0.1$ and $G_{\eta i}(\omega) = 0.2$.
- $\omega_0 = 0.01$ Hz, $\omega_1 = 0.5$ Hz, $\omega_2 = 10$ Hz.
- $\varepsilon_0 = 1.1885$ (1.5 dB), $\varepsilon_1 = 1$ (0 dB), $\varepsilon_2 = 3.162 \times 10^{-3}$ (-50 dB).

Using the pole parameterization, the initial values are set as $r_k = -1$, $\forall\, k \in \{1,2,3,4\}$. Three results are obtained for each combination of the four poles.

- Four real poles ($r_k = -1.3648$, $\forall\, k \in \{1,2,3,4\}$).
- Two real poles ($r_1 = r_2 = -0.2609$) and a conjugate pair ($-2.0004 \pm 2.2374 j$).
- Two conjugate pairs ($r_1 = r_3 = -1.3648$ and $r_2 = r_4 = 0$). This result is the same as the four real pole case.

Since the results of four real poles and two conjugate pairs converge, there are only two different results left. The corresponding $\overline{|\mathbb{T}_{di}|}$ curves are plotted in Fig. 6. The second pole combination (two real poles and one conjugate pair) gives the lowest peak of $\overline{|\mathbb{T}_{di}|}$ (3.1797 dB).

Using the denominator parameterization, the optimized parameters are $a_3 = 4.4840$, $a_2 = 11.1637$, $a_1 = 4.6465$, and $a_0 = 0.6173$. The corresponding $\overline{|\mathbb{T}_{di}|}$ curve is plotted in Fig. 7. The peak value is 3.1522 dB, which is lower than the pole parameterization method.

Note that the optimization process in Matlab does not guarantee the existence of the solution. Therefore, the initial values of the optimization process should satisfy all the constraints. The two parameterization methods give different results. This is because the optimization process in Matlab does not guarantee global optimum. One way to further improve the optimization performance is to iteratively run

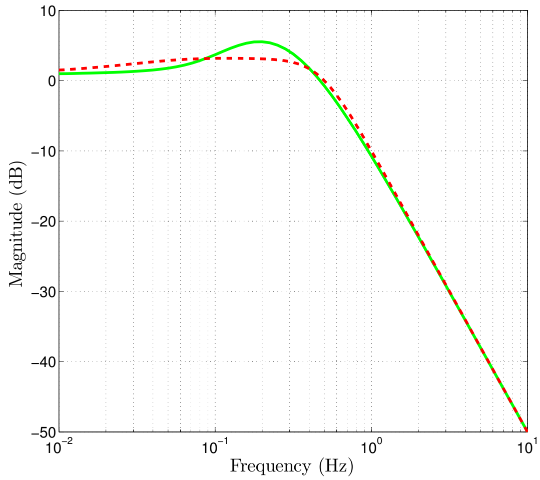

Fig. 6. Optimized $\overline{|\mathbb{T}_{di}|}$ using the pole parameterization. The solid line (green) is the result of four real pole parameterization and the two conjugate pair parameterization. The dashed line (red) is the result of two real poles & a conjugate pair parameterization.

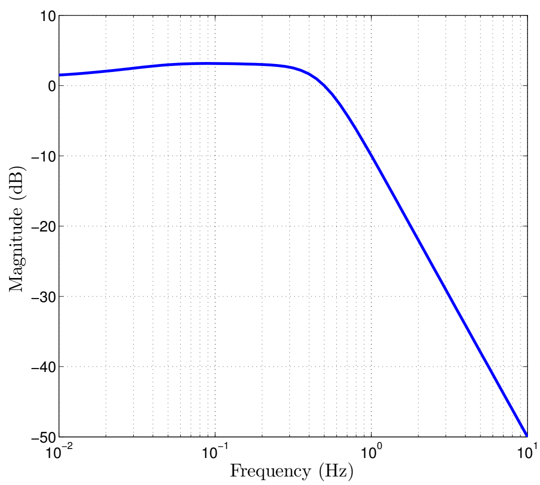

Fig. 7. Optimized $\overline{|\mathbb{T}_{di}|}$ using the denominator parameterization.

the optimization process using the result of the previous optimization process as the initial values. But the improvement gained by using this iteration is usually ignorably small in practice. Nevertheless, the optimization process gives much better result than the manual pole placement.

V. Conclusion

The strategy of combining modal decomposition and frequency-shaped sliding surface control is applied to the 6-DOF AVIS with the measurement scheme of relative displacement and payload absolute acceleration. The 6-DOF AVIS can be decoupled by modal decomposition under the condition of the proportional damping. If this condition is not satisfied, static optimal decoupling [13] can be applied.

The frequency-shaped sliding surface control is described more generally as a two-step control methodology. The first step is to design the sliding surface based on the measurement schemes of relative displacement and payload absolute acceleration. The sliding surface can be designed by numerically solving the transmissibility optimization problem based on the power spectrum of the modal sensor noises and base-frame vibrations. The second step is to realize the optimized performances by the regulator design. To realize the optimized transmissibility, the regulator gain has to be high enough at interested frequencies. The regulator gain is preferred to be low at high frequencies to deal with the possible time delay and unmodeled flexible modes.

This strategy is applicable to a class of multi-DOF AVIS. The advantage with respect to the H_∞ control is that the low implementation cost and the straight-forward design process. The transmissibility optimization process gives the best realizable transmissibility under the conditions of performance constraints, power spectrum of sensor noises, and power spectrum of base-frame vibrations. This strategy is going to be tested in experiments in the near future.

VI. Acknowledgments

This work is a part of the Dutch IOP-EMVT program and is supported financially by SenterNovem, an agency of the Dutch Ministry of Economic Affairs.

References

[1] K. Watanabe, S. Hara, Y. Kanemitsu, T. Haga, K. Yano, T. Mizuno, and R. Katamura, "Combination of H_∞ and PI control for an electromagnetically levitated vibration isolation system", *Proc. 35th Conf. on Decision and Control*, Kobe, Japan, Dec. 1996.

[2] C. Ding, J.L.G. Janssen, A.A.H. Damen, and P.P.J. van den Bosch, "Modeling and control of a 6-dof contactless electromagnetic suspension system with passive gravity compensation", *Proc. XIX Int. Conf. on Electrical Machines*, Rome, Italy, Sep. 2010.

[3] C. Ding, A.A.H. Damen, and P.P.J. van den Bosch, "Stabilization and vibration isolation of a contactless electromagnetic isolator: a frequency-shaped sliding surface control approach", *Proc. Int. Conf. on Advanced Intelligent Mechatronics*, Montreal, Canada, Jul. 2010.

[4] L. Zuo and J.J.E. Slotine, "Robust vibration isolation via frequency-shaped sliding control and modal decomposition", *Journal of Sound and Vibration*, vol. 285, no. 4-5, pp. 1123-1149, 2005.

[5] D. Karnopp, "Active and semi-active vibration isolation" *Journal of Mechanical Design*, vol. 117, pp. 177-185, 1995.

[6] K.D. Young and U. Ozguner, "Frequency shaping compensator design for sliding mode", *Int. Journal of Control*, vol. 57, no. 5, pp. 1005-1019, 1993.

[7] H. Elmali, M. Renzulli, and N. Olgac. "Experimental comparison of delayed resonator and PD controlled vibration absorbers using electromagnetic actuators", *Journal of Dynamic Systems, Measurement, and Control, Trans. of the ASME*, vol. 122, pp. 514-520, 2000.

[8] M. Heertjes, K. de Graaff, and J.G. van der Toorn, "Active vibration isolation of metrology frames; a modal decoupled control design", *Journal of Sound and Acoustics-Trans. of the ASME*, vol. 127, Issue 3, pp. 223-233, 2005.

[9] J.L.G. Janssen, J.J.H. Paulides and E.A. Lomonova, "Passive limitations for a magnetic gravity compensator", *Journal of System Design and Dynamics*, vol. 3, no. 4, pp. 671-680, 2009.

[10] K.D. Young, V.I. Utkin, and U. Ozguner, "A control engineer's guide to sliding mode control", *IEEE Trans. on Control Systems Technology*, vol. 7, no. 3, pp. 328-342, 1999.

[11] M. Serrand and S.J. Elliott, "Multichannel feedback control for the isolation of base-excited vibration", *Journal of Sound and Vibration*, vol. 234, no. 4, pp. 681C704, 2000.

[12] A. Barzilai, T. VanZandt, and T. Kenny, "Technique for measurement of the noise of a sensor in the presence of large background signals", *Review of Scientific Instruments*, vol. 69, no. 7, pp. 2767-2772, 1998.

[13] D. Vaes, K. Engelen, J. Anthonis, J. Swevers, and P. Sas. "Multivariable feedback design to improve tracking performance on tractor vibration test rig", *Mechanical Systems and Signal Processing*, vol. 21, pp. 1051-1075, 2007.